



**HAL**  
open science

## Lewis acido-basic interactions between CO<sub>2</sub> and MgO surface: DFT and DRIFT approaches

Damien Cornu, Hazar Guesmi, Jean-Marc Krafft, H el ene Lauron-Pernot

► **To cite this version:**

Damien Cornu, Hazar Guesmi, Jean-Marc Krafft, H el ene Lauron-Pernot. Lewis acido-basic interactions between CO<sub>2</sub> and MgO surface: DFT and DRIFT approaches. *Journal of Physical Chemistry C*, 2012, 116 (11), pp.6645-6654. 10.1021/jp211171t . hal-01054618

**HAL Id: hal-01054618**

**<https://hal.science/hal-01054618v1>**

Submitted on 7 Aug 2014

**HAL** is a multi-disciplinary open access archive for the deposit and dissemination of scientific research documents, whether they are published or not. The documents may come from teaching and research institutions in France or abroad, or from public or private research centers.

L'archive ouverte pluridisciplinaire **HAL**, est destin ee au d ep ot et  a la diffusion de documents scientifiques de niveau recherche, publi es ou non,  emanant des  tablissements d'enseignement et de recherche fran ais ou  trangers, des laboratoires publics ou priv es.

**Lewis Acido-Basic Interactions Between CO<sub>2</sub> and MgO  
Surface: DFT and DRIFT Approaches**

|                               |  |
|-------------------------------|--|
| Journal:                      | <i>The Journal of Physical Chemistry</i>   |
| Manuscript ID:                | jp-2011-11171t.R1  |
| Manuscript Type:              | Article  |
| Date Submitted by the Author: | n/a  |
| Complete List of Authors:     | Hazar, Guesmi; CNRS/university PARIS VI, Chemistry<br>Lauron-Pernot, H  l  ne; University Paris 06, Laboratoire de r  activit   de surface<br>Damien, Cornu; University Paris 06, Laboratoire de r  activit   de surface<br>Krafft, Jean-Marc; University Paris 06, Laboratoire de r  activit   de surface |
|                               |  |

SCHOLARONE™  
Manuscripts

# Lewis acido-basic interactions between CO<sub>2</sub> and MgO surface: DFT and DRIFT approaches

*Damien Cornu<sup>1</sup>, Hazar Guesmi<sup>1,2\*</sup>, Jean-Marc Krafft<sup>1,2</sup> and H el ene Lauron-Pernot<sup>1</sup>*

<sup>1</sup>UPMC - Universit e Pierre et Marie Curie, Laboratoire de R eactivit e de Surface, UMR 7197, 3 rue Galil e 94200 Ivry sur Seine, France

<sup>2</sup>CNRS, UMR 7197, Laboratoire de R eactivit e de Surface, 3 rue Galil e 94200 Ivry sur Seine, France. Email : hazar.guesmi@upmc.fr

## Abstract

Combined experimental infrared (IR) and theoretical approaches have been carried out in an attempt to specify the actual structure of the CO<sub>2</sub> species adsorbed on the magnesium oxide surface. The interaction of CO<sub>2</sub> with regular sites of the MgO(100), (111) and (110) surfaces as well as MgO(100) defect sites (steps, corners, kinks and di-vacancies) has been investigated by mean of Density Functional Theory study. Theoretical IR frequencies compared with IR experiments show distinguishable carbonate species, adsorbed on different planes and defects, vibrating in different IR-frequency ranges. In addition, by mean of thermodynamic model, the stability of carbonates as a function of temperature have been calculated and compared to the experiment. Analyzing the nature of basic sites, the results show that the most active site versus CO<sub>2</sub>, which is a Lewis acid, is not the same that the strongest site for the deprotonating adsorption of Br onsted acids. The present work revisits and improves the understanding of carbonate species that could exist on the magnesium oxide surface and gives a picture of the accessible planes of magnesium oxide as well as their surface Lewis basicity.

Keywords: MgO(111), MgO(110),MgO(100), defects, charge density difference, thermodynamic calculation, Lewis basicity, Infra-red.

## 1. Introduction

Due to environmental questions, the interest for developing the use of basic catalysts is increasing [1-2]. One of the main drawbacks of these basic catalysts is that they are naturally polluted by water and carbon dioxide forming, by the way of an acid-base reaction, hydroxyl and carbonate groups on the catalyst surface. These adsorbates are usually considered as poisons of the reactivity even if they can be desorbed at specific temperatures depending on their nature and local environment [3]. In order to understand the catalytic properties of the basic catalysts linked to the pretreatment conditions, it is important to be able to characterize the adsorbates remaining on the surface before the catalytic reaction and, as a consequence, to know which basic sites are available after the thermal treatment.

Such an attempt has already been made with hydroxyl groups of magnesium oxide [4-5] which is a well-known basic catalyst involved in numerous studies of industrial interest [3, 6-9]. The aim of this paper is to investigate, by a mixed experimental-theoretical approach, the nature of the carbonates formed by interaction with  $\text{CO}_2$  on MgO surface defects and their stability upon thermal treatment. As  $\text{CO}_2$  is a Lewis acid while  $\text{H}_2\text{O}$  or methanol used in previous studies are Brønsted acidic molecules, the discussion of the results will involve a comparison between Lewis and Brønsted basic properties of MgO.

Infra-Red spectroscopy is one of the more informative techniques for the characterisation of adsorbed molecules [10], as carbonate species, formed on MgO surfaces [11-19]. The literature describes the carbonates present on MgO surface as monodentates or bidentates, but their detailed pictures have been unclear so far and the interpretation of IR band spectra and their attributions in connection to specific adsorbed species are questions which are far from being resolved [2]. In this work, using DRIFT spectroscopy we have followed, for different temperature ranges, the interaction of  $\text{CO}_2$  with MgO powder sample, prepared by precipitation. The originality of the pre-treatment operated here resides in covering the surface

1  
2  
3 previously cleaned up from hydroxyl and carbonates groups by different amounts of CO<sub>2</sub>. In  
4  
5 addition, we have attempted to specify adsorbed CO<sub>2</sub> species by ab-initio DFT method. The  
6  
7 theoretical investigation of CO<sub>2</sub> interactions with MgO surface has often concerned (100) flat  
8  
9 surface [20-22], step and corner defects [20, 22-23]. Due to their lower stability compared to  
10  
11 the (100) surface, the (110) [24] and (111) [23] lattice planes have attracted much less  
12  
13 attention. Nevertheless, as the adsorption of molecules such as water or CO<sub>2</sub> can modify the  
14  
15 relative stabilities of the lattice planes [25], this work presents results obtained on all these  
16  
17 surfaces and also includes kinks and divacancies which can be formed on the (100) surface.  
18  
19  
20  
21

22 In the following the configuration and energetic stability as well as electronic structures of  
23  
24 the different carbonate species which could be formed over MgO support are investigated  
25  
26 using DFT calculations. In addition by mean of thermodynamic model, the stabilities of  
27  
28 carbonates are drawn as a function of temperature. Thus the comparison of DFT calculated  
29  
30 frequencies and measured IR data leads to a detailed description of the surface state  
31  
32 depending on the temperature treatment.  
33  
34  
35  
36  
37  
38  
39  
40  
41  
42  
43  
44  
45  
46  
47  
48  
49  
50  
51  
52  
53  
54  
55  
56  
57  
58  
59  
60

## 2. Experimental and Computational details

### 2.1. Materials and experiments

**2.1.1. Preparation of the catalyst:** Mg(OH)<sub>2</sub> was obtained from Mg(NO<sub>3</sub>)<sub>2</sub> (Aldrich, 99.99%) solution using ammonium hydroxide (Aldrich, 99%) (8 mol.L<sup>-1</sup>) as precipitating agent. Thus, the latter was added to a magnesium nitrate solution (1 mol.L<sup>-1</sup>) and the pH value adjusted to 10 at 303 K. After stirring for 30 min, the precipitate was washed several times with deionized water, and then filtered. The hydroxide sample was finally treated in vacuum (10<sup>-6</sup> Torr) up to 1273 K (ramp 1 K.min<sup>-1</sup>) and maintained at this temperature for 2 h.

**2.1.2. Thermal treatments:** Figure 1 reports the different steps of the thermal treatments of the magnesium oxide sample. During the pre-treatment phase, the sample is “cleaned up” 2h at 1023 K under nitrogen flow (Air Liquide, U nitrogen >99.995% pure) (20 cm<sup>3</sup>.min<sup>-1</sup>), then cooled down to 323 K. During the treatment phase, the sample is first contacted with carbon dioxide (Air Liquide, Alphagaz, >99.9% pure) diluted in nitrogen (5% in a 20 cm<sup>3</sup>.min<sup>-1</sup>.flow) for 15 min. Then, it is once again heated at intermediate temperature (473 K < *temp* < 1073 K) in a nitrogen flow (20 cm<sup>3</sup>.min<sup>-1</sup>) for 2 h. In the following, only the final temperature “*temp*” that determines the degree of carbonatation of the sample will be indicated.

Insert Figure 1

**2.1.3. Spectroscopic measurement:** DRIFT spectra were recorded on a Brüker IFS 66 V spectrometer in the 4000–600 cm<sup>-1</sup> range (4 cm<sup>-1</sup> resolution, 256 scans/spectrum) using a Thermo Spectra-Tech high temperature cell. All spectra were converted into Kubelka–Munk

1  
2  
3 units after subtraction of the spectrum recorded on dehydrated KBr sample. All spectra are  
4  
5 recorded in situ after the pretreatment procedure described in section 2.1.2 and the cooling  
6  
7 down of the sample to 333K. Finally, Raman spectra were recorded on a Model HL5R of  
8  
9 Kaiser Optical System Inc. in the the 3450–100  $\text{cm}^{-1}$  range (4  $\text{cm}^{-1}$  resolution). It is equipped  
10  
11 with a high-powered near-IR laser diode working at 785 nm.  
12  
13  
14

## 15 16 **2.2. Computational details**

17  
18  
19  
20 **2.2.1. Methods.** All calculations were performed using *ab-initio* plane-wave pseudopotential  
21  
22 approach as implemented in VASP [26-27]. The generalized gradient approximation  
23  
24 exchange-correlation functional of Perdew and Wang PW91 [28] was chosen to perform the  
25  
26 periodic DFT calculations with reliable accuracy on the convergence criterions. The one  
27  
28 electron wave function was developed on a basis set of plane waves and the interaction  
29  
30 between the core and the valence electrons is described by the projector augmented waves  
31  
32 (PAW) approach [29]. The selected description of the oxygen atomic core allows a good  
33  
34 convergence on the energy for a cutoff of 400 eV. The convergence criterion for the  
35  
36 electronic self-consistent cycle was fixed to  $10^{-6}$  eV per supercell. Geometry optimizations  
37  
38 were performed within a conjugate-gradient algorithm until the convergence criterion on  
39  
40 forces ( $10^{-2}$  eV.Å<sup>-1</sup>) was reached. A dipolar correction along the perpendicular to the slab was  
41  
42 applied in order to remove the effect of electrostatic interaction between the slab and its  
43  
44 periodic images along the *z* axis. The adsorption energy of carbonates on the MgO surfaces  
45  
46 was calculated as:  
47  
48  
49  
50  
51

$$52 \quad E_{\text{ads}}(\text{OK}) = E_{\text{CO}_2/\text{surf}} - (E_{\text{surf}} + E_{\text{CO}_2\text{free}}) \quad \text{eq. 1}$$

53  
54  
55 Where  $E_{\text{surf}}$  represents the energy of bare surface,  $E_{\text{CO}_2\text{free}}$  is the energy of CO<sub>2</sub> gas and  
56  
57  $E_{\text{CO}_2/\text{surf}}$  that of the adsorbed system.  
58  
59  
60

1  
2  
3 Vibrational spectra were calculated for selected surface species within the harmonic  
4 approximation. In addition to CO<sub>2</sub> molecules, magnesium and oxygen surface atoms in direct  
5 interaction with adsorbed species were allowed to relax. The Hessian matrix was computed by  
6 the finite difference method followed by a diagonalization procedure. The eigenvalues of the  
7 resulting matrix lead to the frequency values. The assignment of the vibrational modes is done  
8 by inspection of the corresponding eigenvectors. Free carbon dioxide molecule is used as a  
9 reference in order to estimate the systematic deviation between experimental and calculated  
10  $\nu_{\text{CO}}$  values. The DFT calculated vibration frequencies for free CO<sub>2</sub> are 2366 (2349),  
11 1318(1340) and 637(667) cm<sup>-1</sup> (experimental frequencies [30] are indicated in parenthesis).  
12 As the average of calculated frequencies fit quite well the average experimental values, no  
13 empirical scaling factors were applied to the DFT reported frequencies.  
14  
15  
16  
17  
18  
19  
20  
21  
22  
23  
24  
25  
26  
27  
28  
29  
30

### 31 **2.2.2. Surfaces.**

32  
33 The computed models representing MgO (100) irregularities such as monatomic steps (S1),  
34 diatomic steps (S2), corners (C3), divacancies (D), and kinks (K), used in this work, were the  
35 same ones that were already considered by C. Chizallet and H. Petitjean et al. regarding the  
36 interaction of water [4-5] and methanol molecules [31]. The MgO (100) terrace (T) involving  
37 five coordinated oxygen ions (O<sup>2-</sup><sub>5C</sub>) was modelled by considering a slab formed by 5 layers  
38 where only the 3 topmost ones were allowed to relax during optimization process. Each layer  
39 was formed by 8 MgO pairs and was separated from the other by optimized distance of 2.13 Å.  
40  
41 The MgO (110) surface consists of alternating rows of Mg and O ions. The slab was formed  
42 by 6 layers and only the 4 topmost layers were allowed to relax. The rows were 6 dMg-O of  
43 length and were separated by optimized distance of 3.01 Å.  
44  
45  
46  
47  
48  
49  
50  
51 The MgO (111) surface was modelled by repeated slab of 12 layers. Because we are  
52 interested here into the formation of carbonate species by interaction of CO<sub>2</sub> with the oxide  
53  
54  
55  
56  
57  
58  
59  
60



1  
2  
3 surface, we have limited our investigation to the oxygen terminated rocksalt (111) surface  
4  
5 model. The central 6 atomic layers (including 3 Mg and 3 O layers) were kept fixed in the  
6  
7 structure optimization process and the other top most layers were free to relax. To avoid  
8  
9 artificial surface-surface interactions, the vacuum between the repeated slabs was fixed to 20  
10  
11 Å. We have tested that our optimized properties as surface atomic distances and inter-planar  
12  
13 distances between O and Mg close-packed (111) planes are in line with previous reliable  
14  
15 models used in the literature [32-33].  
16  
17

18  
19 The Brillouin zone integrations are performed on a Monkhorst-Pack 2x1x1  $k$  point mesh for  
20  
21 (100) surface and defects and 2x2x1  $k$  point mesh for (110) and (111) surfaces. For MgO  
22  
23 (100), (110) and (111) surfaces, we have checked that the calculated average surface energies  
24  
25 for each surface orientation are comparable to literature values [34-36]. As expected, the  
26  
27 calculated surface energy for the (111) facet was found to be relatively high ( $5.3 \text{ J.m}^{-2}$  ( $4.16$   
28  
29  $\text{J.m}^{-2}$  [34])) compared to (110) facet ( $2.2 \text{ J.m}^{-2}$  ( $2.18 \text{ J.m}^{-2}$  [34])) and (100) facet ( $1.73 \text{ J.m}^{-2}$   
30  
31 ( $1.29 \text{ J.m}^{-2}$  [34])). This difference reflect well the instability of the polar terminated surface  
32  
33 compared to the (100) one.  
34  
35  
36  
37  
38  
39

### 40 41 **2.2.3. Thermodynamic**

42  
43 In order to study the adsorption phase diagram of  $\text{CO}_2$  molecule on the different considered  
44  
45 surfaces, a model of atomistic thermodynamics was developed. This model was inspired from  
46  
47 the one developed by D. Loffreda et al. [37] for a realistic description of adsorption  
48  
49 thermodynamics of multifunctional molecules on metal surfaces.  
50  
51

52  
53 The Gibbs free adsorption energy depends on the adsorption internal energy and on the  
54  
55 vibrational entropy change during the adsorption process. Thus, for an accurate description of  
56  
57 the free Gibbs energy, the vibrational contributions of the initial (bare surface and gas phase)  
58  
59  
60

and final system (adsorbed system) should be included in the formalism. In this work the Gibbs free adsorption energy was calculated as follows:

$$\Delta G_{ads} = \Delta E_{ads} + \Delta E_0 + T(\Delta S_{vib} + \Delta S_{trans,rot} + S_{config}) - kT \ln(P/P_0) \quad \text{eq. 2}$$

Where  $\Delta E_{ads}$  is the adsorption energy calculated from DFT (see eq. 1),  $\Delta E_0$  is the zero point energy (ZPE) change during adsorption process and  $\Delta S_{vib}$ ,  $\Delta S_{trans,rot}$  are the vibrational and transitional, rotational entropy changes, respectively. The calculated vibrational properties in carbonated systems included the interacting molecule and all top-most surface atoms. Similarly for decarbonated systems the first surface layer was considered.

When several adsorption sites ( $N_{site}$ ) are available on the surface, an additional term called configurational or positional entropy,  $S_{config}$  is included in the formalism. It defines the logarithm of all possible arrangements of the molecule on the surface. Its value is given by the equation 3.

$$S_{config} = -k \ln \left[ \frac{N_{site}!}{(N_{site} - N_{ads})! N_{ads}!} \right] \quad \text{eq. 3}$$

Finally,  $\Delta S_{vib}$  is derived from the reduced vibrational partition functions  $Q^{vib}$  of adsorbate system, gas phase and surfaces (eq. 4) and  $\Delta S_{trans,rot}$  is calculated (eq. 5) on the basis of the transitional partition function of the adsorbate system  $Q_{ads}^{trans}$  and the gas phase  $Q_{gas}^{trans}$  as well as the rotational partition function of gas phase  $Q_{gas}^{rot}$ .

$$\Delta S_{vib} = -k \ln \left( \frac{Q_{ads}^{vib}}{Q_{surf}^{vib} Q_{gas}^{vib}} \right) \quad \text{eq. 4}$$

$$\Delta S_{trans,rot} = -k \ln \left( \frac{Q_{ads}^{trans}}{Q_{gas}^{trans} Q_{gas}^{rot}} \right) \quad \text{eq. 5}$$

### 3. Results and discussion

#### 3.1. Experimental IR data

The effect of the pretreatment (1023 K, 2h under N<sub>2</sub>) on the adsorbed species over MgO surface is shown by the comparison of the DRIFT spectra of the initial sample and of the treated one (Figure 2). The considered high temperature process cleans up the surface from almost all hydroxides and carbonates. The IR spectra (black line) shows a weak remaining absorption band at 3750 cm<sup>-1</sup> which is attributed to strongly bounded hydroxides [5], and some carbonates with IR bands at 1657 and 1329 cm<sup>-1</sup>.

Insert Figure 2

After the addition of CO<sub>2</sub>, DRIFT data show strong modifications in the IR range 1800- 1000 cm<sup>-1</sup>. Figure 3 gathers the set of IR spectra obtained after the surface treatments at temperatures *temp* = 523 K, 673 K, 873 K. As expected, the spectra show the formation of carbonate species the amount of which decreases upon the successive thermal treatments. After the treatment at 873 K, the obtained spectra show the same absorption in the 1000 – 2000 cm<sup>-1</sup> range as the one recorded after the pre-treatment at 1023 K. In addition, the successive thermal treatments (*temp*) do not affect the recorded high frequencies (> 2000 cm<sup>-1</sup>) on magnesium dioxide surface. In the lower frequency ranges, the absorptions are always very high due to the bulk infrared absorption of MgO with a lateral phonon frequency at 800 cm<sup>-1</sup> [38].

Insert Figure 3

According to the literature, adsorption of carbonate species leads to the splitting of the  $\nu_3$  stretching vibration band of the free ion, located at 1415 cm<sup>-1</sup>, and gives different contributions depending on the geometry of the adsorbed ion [2,13]. The carbonate  $\nu_3$

1  
2  
3 stretching mode is split to  $\nu_{3\text{high}}$  and  $\nu_{3\text{low}}$  contributions. Generally a consensus is gained that  
4  
5 the more coordinated the carbonate ion the more split the two contributions. In addition the  
6  
7 average  $\Delta\nu$  for each species has also been determined [13]. As reported in Table 1, which  
8  
9 summarizes the IR results from numerous experimental studies, the vibrational frequency  
10  
11 bands recorded on magnesium oxide surfaces have been assigned either to monodentate,  
12  
13 bidentate or hydrogen carbonate species [11-12, 14-16, 18]. This table also evidences many  
14  
15 discrepancies relative to the IR values assigned to different carbonate species, which may be  
16  
17 due to the different states of the MgO surfaces obtained after the thermal treatment such as  
18  
19 hydration state, morphology etc...  
20  
21  
22  
23  
24  
25

26 Insert Table 1  
27  
28

29 In this work (see figure 3), MgO surface is almost free of residual adsorbates. Therefore no  
30  
31 hydrogen carbonate can be found on the surface even at  $temp = 523$  K (no contribution at  
32  
33  $1220\text{ cm}^{-1}$ ). Comparing the position of our recorded spectra with IR attributions reported in  
34  
35 Table 1, one can assign, “at first sight”, all the identified bands in the range of  $1370\text{--}1590\text{ cm}^{-1}$   
36  
37 to monodentate species and those in the ranges of  $1270\text{--}1390\text{ cm}^{-1}$  and  $1620\text{--}1710\text{ cm}^{-1}$  to  
38  
39 bidentate species. Moreover, two minor contributions located at  $1252$  and  $1275\text{ cm}^{-1}$  do not  
40  
41 change with the thermal treatment and can be linked to the small amount of silicon which is a  
42  
43 residual impurity in the sample. This attribution of the carbonate bands goes on line with the  
44  
45 evolution of the spectra with  $temp$ : the most stable species are reported as bidentate [11] and  
46  
47 are the only ones remaining on MgO surface after a treatment at  $873$  K, giving contributions  
48  
49 at  $1661\text{ cm}^{-1}$  and  $1321\text{ cm}^{-1}$ . Nevertheless, for each carbonate species, several contributions  
50  
51 are obtained. For instance, in the infrared range attributed to bidentate species, two bands at  
52  
53  $1680$  and  $1651\text{ cm}^{-1}$  (split bands at  $1321$  and  $1304\text{ cm}^{-1}$ ) can be attributed to two different  
54  
55 bidentate species. The same analysis can be made with the monodentate species. These  
56  
57  
58  
59  
60

1  
2  
3 different contributions are probably linked to the carbonate formation on different MgO  
4  
5 defects. Because in catalytic applications these defects may behave differently [39-41] it is  
6  
7 important to know which of them are poisoned by carbonates as a function of the thermal  
8  
9 treatment process. Modelling is thus necessary to calculate the theoretical position of the IR  
10  
11 band linked to carbonates species depending on their topological environment.  
12  
13  
14  
15  
16  
17

## 18 **3.2. Computational results**

### 19 **3.2.1. On the nomenclature of carbonates**

20  
21  
22 The earlier work of Fukuda and Tanabe [11] described the carbonates as “bidentate” or  
23  
24 “unidentate” for the carbonate linked with only one magnesium ion, and “bridging” for the  
25  
26 one bonded with two magnesium ions (see scheme 1). Busca and Lorenzelli [13] added some  
27  
28 complexity to this model by considering “polydentate” species. The improvement in the  
29  
30 description of the carbonates by the way of computational methods allows us to give a more  
31  
32 precise description of the carbonates. Those carbonate should be given an unambiguous name.  
33  
34 We propose that the carbonates should be ranked by the number of oxygen atoms making  
35  
36 connection with the surface (ionic or covalent bonds), such connections being the bonds that  
37  
38 lengths are less or equal to the Mg-O bond length in the bulk magnesium oxide ( $\approx 2.1 \text{ \AA}$ ). Let  
39  
40 us add that a thorough description of the nature of carbonate bonds will be evaluated through  
41  
42 DFT electronic analysis. Thus, mono-, di- and tri-dentate carbonates refer, from now on, to  
43  
44 carbonate species in which one, two and three oxygen atoms are connected to the surface,  
45  
46 respectively. In addition among a general type of carbonate species, for example bidentate,  
47  
48 distinctions will be made considering the type of plan or surface defect on which the  
49  
50 interaction occurs. The carbonates will be named by the combination of a letter for each type  
51  
52 (M : monodentate, B : bidentate, T : tridentate) and of the name of defect or plane. For  
53  
54  
55  
56  
57  
58  
59  
60

1  
2  
3 instance, T-S1 will refer to a tridentate carbonate formed on a S1 step, and M-(111) will  
4  
5 refers to a monodentate carbonate on a (111) plane.  
6  
7

8 Inset scheme 1  
9

### 10 11 **3.2.2. CO<sub>2</sub> species adsorbed on MgO(100) surface** 12

13  
14  
15 In table 2 are reported geometric and energetic parameters as well as  $\nu_{\text{CO}}$  frequencies of all  
16  
17 optimized configurations of CO<sub>2</sub> species adsorbed on the MgO (100) plane and its various  
18  
19 defects (mono (S1) and diatomic steps (S2), corner (C3), kink (K) and divacancy (D)).  
20  
21 Comparisons with available values from the literature are also considered [14, 20, 22-24].  
22  
23

24  
25 Inset Table 2  
26  
27

28  
29 *Adsorption on the flat surface:* The low calculated adsorption energy (-0.09 eV) for linear  
30  
31 CO<sub>2</sub> molecule on flat (100) terraces T confirms that five coordinated O<sup>2-</sup><sub>5C</sub> ions of MgO  
32  
33 surface are totally unreactive for the formation of carbonates in agreement with literature data  
34  
35 [21, 42].  
36  
37

38  
39 *Adsorption on surface defects:* DFT calculations of CO<sub>2</sub> interactions with four and three  
40  
41 coordinated oxygen ions (O<sup>2-</sup><sub>4C</sub> and O<sup>2-</sup><sub>3C</sub>), involved in the defects of the MgO(100) plan,  
42  
43 show largely more stable adsorbed carbonate species compared with flat MgO(100), (Table  
44  
45 2). Pacchioni has investigated the interaction of CO<sub>2</sub> on regular and defect sites of the  
46  
47 MgO(100) surface by mean of *ab-initio* cluster model SCF calculations [42]. He explained  
48  
49 that because of the considerably large Madelung potential of a surface five coordinated  
50  
51 oxygen ion (O<sup>2-</sup><sub>5C</sub> site) compared to the lower coordinated site as the four coordinated O<sup>2-</sup><sub>4C</sub>  
52  
53 sites, the electron cloud of the O<sup>2-</sup><sub>4C</sub> ion is more spatially diffuse and can easily overlap with  
54  
55 the CO<sub>2</sub> empty orbitals interacting with the surface.  
56  
57  
58  
59  
60

Inset Figure 4

1  
2  
3 DFT optimizations predict that CO<sub>2</sub> molecule adsorbs with energy values of -2.26 and -2.16 eV  
4  
5 on the S1 and S2 step systems, respectively (Figures 4.a and 4.b). The molecule interacts with  
6  
7 O<sup>2-</sup><sub>4C</sub> ions with an average d<sub>C-O</sub> distance of 1.37 Å and assumes an orientation “parallel” to the  
8  
9 edge which allows a direct electrostatic interaction of its O atoms with the Mg<sup>2+</sup><sub>4C</sub> cations of  
10  
11 the surface. The O-C-O angle is predicted to be of about 130°. These results are in line with  
12  
13 those of Olsbye and co-workers [20] who have called a similar configuration of adsorbed  
14  
15 carbonate species as “monodentate”. Nevertheless, as in a such configuration the carbonate  
16  
17 species form three connections (short bonds < 2.10 Å) with the MgO surface (one O<sup>2-</sup> is  
18  
19 already inserted in the magnesium oxide network (O<sub>β</sub>) and two Mg<sup>2+</sup> are linked to the  
20  
21 oxygen ions (O<sub>α</sub>) of CO<sub>2</sub>). Thus we propose (see section 3.2.1) to call them as tridentate  
22  
23 carbonates (T-S1 and T-S2).  
24  
25  
26  
27  
28

29 One way in which one can gain further insight into the molecule/surface interactions as well  
30  
31 as the character of the bonding from the results of the DFT calculations is to investigate the  
32  
33 change in the electron density distribution in the surface as a result of the adsorbate bonding.  
34  
35 This can be reached by calculating the difference charge electron density obtained by  
36  
37 subtracting from the charge electron density of the adsorbed carbonate system both the charge  
38  
39 electron density of the clean MgO surface and that of an isolated CO<sub>2</sub>. The atomic positions of  
40  
41 the clean surface and of the isolated gas are taken to be the same as those of the relaxed  
42  
43 adsorbate system [43]. Figure 5 depicts the *charge density difference* of computed carbonate  
44  
45 species graphically represented [44] by isosurface contours. These 3D visualizations reveal  
46  
47 that all relevant chemical changes are suffered by the O valence of carbonates. Concerning the  
48  
49 T-S1 configuration, there is clearly evidence of three connections occurring between  
50  
51 carbonate and the edge of the MgO step. The electron charge appearing into O2p orbitals  
52  
53 pointing towards Mg<sup>2+</sup><sub>4C</sub> cations indicates the formation of two polar covalent bonding. The  
54  
55  
56  
57  
58  
59  
60

1  
2  
3 third connection is the ionic one between ( $O\beta$ ) and the magnesium cations of the oxide  
4  
5 network.  
6

7  
8 Insert Figure 5  
9

10  
11  
12 In order to investigate the effect of coverage on the surface interactions of carbonates we  
13 report in table 3 the calculated adsorption energies of carbonates with increasing coverage.  
14  
15 With respect to the adsorption energy of single T-S1 (S1 surface includes 3 adsorption sites),  
16  
17 the adsorption of a second and a third carbonate is lowered by 1.01 and 1.94 eV, respectively  
18  
19 (the adsorption energies are calculated by considering the surface already adsorbing  $CO_2$   
20  
21 molecules). Because of the strong repulsive interaction between oxygen carbonates, the  
22  
23 second adsorbed T-S1, which has a similar geometry, adopts an orientation shifted with  
24  
25 regard to the first carbonate. In that conformation (see figure 6), one magnesium ion of the  
26  
27 edge is connected to two carbonates and so tries to reach the MgO bulk octahedral geometry.  
28  
29 The calculated Hessian matrix (table 2) of the adsorbed tridentate species indicates  
30  
31 wavenumbers of  $1603\text{ cm}^{-1}$  (T-S1),  $1639\text{ cm}^{-1}$  (T-S2) and  $1300\text{ cm}^{-1}$  (T-S1),  $1287\text{ cm}^{-1}$  (T-S2)  
32  
33 for  $\nu_{3h}$  and  $\nu_{3l}$ , respectively. As shown in table 3, these later frequencies are affected by the  
34  
35 presence of the second and the third neighbouring carbonate surface ( $\theta = 2/3$  and  $\theta = 1$  ML).  
36  
37 Thus, compared to the case of isolated carbonate, the calculated vibrations vary by less than  
38  
39  $100\text{ cm}^{-1}$  for  $\theta = 2/3$ ML and highly change for the monolayer coverage. The split between low  
40  
41 and high frequencies grows when the coverage increases, due to the coupling between the  
42  
43 adsorbed carbonates sharing a  $Mg^{2+}$  cation. Similar results were also observed for  $CO_2$   
44  
45 adsorbed on ZnO surface [45].  
46  
47  
48  
49  
50  
51  
52  
53

54  
55 Insert table 3 and Figure 6  
56

57  
58 Considering these results, the experimental bands (Figures 2 and 3) observed around 1660 and  
59  
60  $1320\text{ cm}^{-1}$ , that remain clearly visible whether the considered temperature, can be attributed to



1  
2  
3 single tridentate species strongly attached on the steps defects of the magnesium oxide  
4  
5 surface.  
6

7  
8 The modelled corner, kink and divacancy systems (Figure 4.c, 4.d, 4.e) involve a three  
9  
10 coordinated ion  $O^{2-}_{3C}$  which interacts directly with the adsorbed  $CO_2$  molecule. On this sites,  
11  
12 the adsorption energy of carbonate species are found to be lower than on the four coordinated  
13  
14 sites. The analysis of the distances between  $O\alpha$  and the surface (table 2) show that carbonates  
15  
16 are doubly bounded to the surface through the network oxygen ( $O\beta$ ) and one oxygen atom  
17  
18 ( $O\alpha$ ) from  $CO_2$ . The bond character of these bidentate carbonates (B-C3, B-K and B-D) can  
19  
20 be analysed from the *charge density difference* graphic represented in figure 5. On the kink  
21  
22 (the same trend is observed for divacancy (not represented)), the adsorption does not strongly  
23  
24 modify the slab. The electron rich zones appearing into  $O2p$  orbitals indicate only one polar  
25  
26 covalent bond between ( $O\alpha$ ) from  $CO_2$  and  $Mg^{2+}_{4C}$ . The electron rich zone around the third  
27  
28 oxygen atom, the ( $O\gamma$ ) of the carbonate molecule, is orientated out of the plane and thus, that  
29  
30 oxygen does not make any connection with the surface. On the corner, the interaction of B-C3  
31  
32 induces a strong modification on the substrate. The surface oxygen atom ( $O\beta$ ) is strongly  
33  
34 displaced in order to insure the double connection of carbonate species with the surface. IR  
35  
36  $\nu_{CO}$  ( $\nu_{3h} - \nu_{3l}$ ) frequencies of carbonates adsorbed on corners, kinks and divacancies, are  
37  
38 calculated to be of  $1727-1198\text{ cm}^{-1}$  (B-C3),  $1679-1125\text{ cm}^{-1}$  (B-K) and  $1649-1149\text{ cm}^{-1}$  (B-D),  
39  
40 respectively. These resulted values can predict that the experimental band observed at  $1680$   
41  
42  $\text{cm}^{-1}$  on the sample treated at  $temp = 523$  and  $673\text{ K}$  is the signature of bidentate carbonate  
43  
44 species adsorbed on corner, kink and/or divacancie defects. The  $\nu_{3l}$  band frequencies are out  
45  
46 of the range of this study. As there is only one adsorption site, the effect of coverage is not  
47  
48 considered here.  
49  
50

51  
52 Finally, it remains the question of the observed IR bands between  $1350$  and  $1600\text{ cm}^{-1}$   
53  
54 (namely located at  $1516\text{ cm}^{-1}$ ,  $1423\text{ cm}^{-1}$  and  $1367\text{ cm}^{-1}$ ) for the sample treated at  $temp = 523$   
55  
56  
57  
58  
59  
60

1  
2  
3 and 673 K which cannot be explained by the presence of carbonate species on the MgO (100)  
4 defects. Moreover, Yanagisawa et al. [14] have already considered the adsorption of CO<sub>2</sub> on  
5 cubic crystallites of the MgO smoke, which exhibit well-defined (100) facets, and they have  
6 not observe any IR adsorption between 1350 and 1600 cm<sup>-1</sup>. This means that the recorded IR  
7 frequencies on our samples would results from different adsorption configurations on other  
8 crystallographic planes even if they are known to be less stable in vacuum conditions  
9 compared to the (100) plane. In fact, several theoretical [34, 46-47] and experimental [48]  
10 studies have shown the change in the stability of surface orientations after the addition of  
11 adsorbates such as water. As IR spectroscopy showed that, in our conditions, few OH groups  
12 remain on the surface, we investigate, in the following section, the adsorption configurations  
13 and properties of CO<sub>2</sub> on faceted (110) and (111) MgO.  
14  
15  
16  
17  
18  
19  
20  
21  
22  
23  
24  
25  
26  
27  
28  
29

### 30 **3.2.3. CO<sub>2</sub> species adsorbed on MgO(111) and (110) surfaces**

31  
32  
33  
34 In figures 4f and 4g are reported the configurations of carbonate species formed over the  
35 modelled MgO(111) and (110) surfaces, respectively. As shown in table 2, the most  
36 energetically stable species (-2.75 eV) is formed over the MgO (110) surface. Over this plan,  
37 the orientations as well as the geometry of carbonates are similar to T-S1 and T-S2; thus, this  
38 carbonate is called tridentate T-110. Therefore, while the *charge density difference* graphic  
39 (figure 5) show similar isosurface shape of the electron rich zones of tridentate species, the  
40 adsorption is energetically favourable, by 0.49 eV, on the (110) than on the stepped (100).  
41 The vibrational frequency calculations of T-110 indicate values at 1559 and 1331 cm<sup>-1</sup> for the  
42  $\nu_{\text{CO}_{3\text{h}}}$  and  $\nu_{\text{CO}_{3\text{l}}}$ , respectively. This carbonate type may correspond to the species vibrating  
43 around 1510 and 1360 cm<sup>-1</sup> on our sample treated at *temp* = 523 and 673 K.  
44  
45  
46  
47  
48  
49  
50  
51  
52  
53  
54  
55  
56  
57  
58  
59  
60

1  
2  
3 As for the stepped (100) surface, in presence of neighbouring carbonates the  $\nu_{\text{CO}}$  strongly  
4 vary and the split between low and high frequencies of T-110 grows as the coverage increases  
5  
6  
7  
8 (Table 3).  
9

10 Over the (111) surface terminated by oxygen atoms, the carbonate lies to the surface through  
11 a single connection. Thus, the carbonates adsorbs as monodentate species on the MgO(111)  
12 surface. In spite of the short  $d_{\text{C-O}(\beta)}$  bond distance of 1.31 Å, which is the same than for the  
13 tridentate configuration, the small O-C-O angle of 115° illustrate the repulsive interactions  
14 that undergoes between the oxygen atoms ( $\text{O}_\gamma$ ) and the surface (Figure 4g). These repulsive  
15 interactions can clearly be attested in figure 5 by the *charge density difference* on M-111  
16 configuration that evidences the low electron density between ( $\text{O}_\gamma$ ) and the surface. This may  
17 explains the low energetic stability of these species. In addition, as the carbonate presents a  
18 symmetry close to  $D_{3h}$ , the split between  $\nu_{\text{CO}_{3h}}$  and  $\nu_{\text{CO}_{3l}}$  is very low: 1440 and 1378  $\text{cm}^{-1}$   
19 (1415  $\text{cm}^{-1}$  for the free carbonate [49]). These values are smaller than the frequency values  
20 calculated by Allen et al [23] who predicted a vibrational frequencies for adsorbed carbonates  
21 on MgO(111) surface in the ranges of 1440 – 1459 and 1572 – 1631  $\text{cm}^{-1}$ . This is probably  
22 due to the empirical method used by these authors. In this work, the resulted monodentate  
23 carbonate, with weekly degenerated IR-band, could be attributed to the species vibrating at  
24 1423  $\text{cm}^{-1}$  on the DRIFT spectra for the sample treated at  $temp = 523$  and 673 K.  
25 Nevertheless, the low bonding energy of -0.8 eV is not consistent with the persistence of the  
26 IR bands for high temperature treatments. This point will be discussed in the next section. In  
27 table 3 are also reported the adsorption energies and  $\nu_{\text{CO}}$  frequency values of carbonate M-  
28 111 for increasing coverage. The high coverage was not reached because of the strong  
29 repulsive interactions occurring between surface/carbonates and carbonate/carbonate species.  
30 Thus, as depicted in table 3, for coverage of 3/4 monolayer the adsorption is highly  
31  
32  
33  
34  
35  
36  
37  
38  
39  
40  
41  
42  
43  
44  
45  
46  
47  
48  
49  
50  
51  
52  
53  
54  
55  
56  
57  
58  
59  
60

1  
2  
3  
4  
5  
6  
7  
8  
9  
10  
11  
12  
13  
14  
15  
16  
17  
18  
19  
20  
21  
22  
23  
24  
25  
26  
27  
28  
29  
30  
31  
32  
33  
34  
35  
36  
37  
38  
39  
40  
41  
42  
43  
44  
45  
46  
47  
48  
49  
50  
51  
52  
53  
54  
55  
56  
57  
58  
59  
60

endothermic and the calculated frequency values are highly different from those of single carbonate calculations.

### 3.2.4. Adsorption thermodynamics

In order to get a more precise picture of the respective stabilities of adsorbed carbon dioxide on different plans and defects and more particularly, to determine the temperature of desorption of the different adsorbed carbonates, the Gibbs free adsorption energy diagram was plotted for each considered system (see figure 7). The partial pressure is set to 0.001 Pa and desorption is presumed to occur when the Gibbs free adsorption energy becomes positive.

Insert Figure 7

As reported in figure 7, Gibbs free adsorption energies of carbonates follow the same linear trend. On the (100) plan, bidentate carbonate species which populate the corners, kinks and divacancies are predicted to leave the MgO support for temperature range of 722-822 K. Tridentate carbonates formed on the Mg(100) steps would desorb at higher temperature and remain on the surface for temperatures as high as 908 K. This is in agreement with the assignment we made for the IR bands recorded at  $temp = 873$  K to highly adsorbed tridentate species

The same kind of tridentate species is also strongly adsorbed on (110) surface thus should not disappear at  $temp < 1200$  K. But experimentally, it is shown that the corresponding IR bands (1516 and 1367  $cm^{-1}$ ) disappear from the spectrum at  $673 < temp < 873$  K. We suppose that this contradiction may be explained considering the well known stability of the (100) surface compared to the (110): surface recombination may thus occur at  $temp < 873$  K, leading to the disappearance of the (110) plane and to the desorption of these species at lower temperature than predicted by our thermodynamic calculations. Moreover, the surface reconstruction of

1  
2  
3 the (110) planes into reconstructed stepped (100) surface [50] may also explain the  
4  
5 enhancement of the IR-adsorption at  $1321\text{ cm}^{-1}$  assigned to T-S1. Let us add that this  
6  
7 reconstruction phenomenon should be confirmed by an appropriate kinetic study.  
8  
9

10 Finally, on the (111) surface, the desorption of monodentate carbonates is predicted to occur  
11  
12 at 314 K. Regarding this result, the IR band observed at  $1440\text{ cm}^{-1}$  for temperature as high as  
13  
14  $temp = 673\text{ K}$  can not be attributed to the monodentate species. Du and co-workers have  
15  
16 attributed similar infrared recorded bands of  $\nu_{\text{CO}_{3\text{h}}} = 1445\text{ cm}^{-1}$  and  $\nu_{\text{CO}_{3\text{l}}} = 1375\text{ cm}^{-1}$  to  
17  
18 bulk-like carbonates which could desorb at high temperature [19]. Mekhemer et al. [17] have  
19  
20 reported similar suggestion. In order to characterize such carbonates, we have performed  
21  
22 Raman spectra on a sample treated at 673 K. Nevertheless, no absorption band at  $1100\text{ cm}^{-1}$ ,  
23  
24 characteristic of the  $\nu_1$  Raman active bulk carbonates [51-52] was observed on this sample. As  
25  
26 bulk carbonates can be present but their amount may be under the detection limit of the  
27  
28 Raman spectrometer, a conclusion on that point is difficult to be made.  
29  
30  
31  
32  
33

### 3.3. New insights on basicity characterization

34  
35 As underlined in the introduction, in order to study the catalysis, we need to know the nature  
36  
37 of the basic sites available after the pretreatment step. For that purpose, the data obtained in  
38  
39 this study on carbonates species, giving their nature, localisation, desorption temperature and  
40  
41 IR vibration bands (calculated and experimentally detected) are summed up in Table 4. The  
42  
43 new nomenclature of these species is also reported in order to take into account not only their  
44  
45 mono-, bi- or tri-dentate character but also the topology of their adsorption site.  
46  
47  
48  
49  
50

51  
52 Insert Table 4  
53

54 Moreover, the literature dealing with basic catalysts reactivity shows that the characterization  
55  
56 of the basic sites is a key point for the interpretation of the catalytic results. One of the most  
57  
58 popular method to determine these basic properties is  $\text{CO}_2$  TPD that consists in following the  
59  
60 progressive desorption of pre-adsorbed  $\text{CO}_2$  with increasing temperature (see as an example,

1  
2  
3 Hattori's review [53]). An attempt to discuss the relevance of this method has already been  
4  
5 made [54] underlining that CO<sub>2</sub> adsorption probes the Lewis basic character of the surface  
6  
7 whereas Brønsted basicity is mainly involved in catalytic reaction. Let us remind that Lewis  
8  
9 basicity is the ability of the surface to give an electronic pair to a Lewis acid molecule while  
10  
11 Brønsted basicity is, according to Brønsted definition [55], the ability to deprotonate a  
12  
13 molecule. It implies that all Lewis bases are also Brønsted bases and reciprocally. But we  
14  
15 demonstrate here, in the particular case of oxides ions, that the strength scale is different  
16  
17 depending on the nature of the considered basicity.  
18  
19  
20

21  
22 This demonstration is made from the comparison of the deprotonating adsorption energy of  
23  
24 water (a Brønsted acid) and the formation of the Lewis adducts of CO<sub>2</sub> (a Lewis acid) on  
25  
26 MgO (100) plane defects. Using similar theoretical approach, C. Chizallet and co-workers  
27  
28 have established the desorption temperature of H<sub>2</sub>O from the MgO (100) defects. According  
29  
30 to these authors water leaves S1, K, D and C3 defects at temperatures of 620K, 805K, 1110K  
31  
32 and 740K, respectively [4]. Thus, it can be seen that the strongest interaction between water  
33  
34 and the surface is achieved on kinks and divacancies whereas the most stabilizing sites for  
35  
36 CO<sub>2</sub> adsorption are predicted here to be the steps. By consequence, direct correlation between  
37  
38 the information obtained by CO<sub>2</sub> TPD and a reaction which first step is a deprotonation has to  
39  
40 be made very cautiously.  
41  
42  
43  
44  
45

#### 46 **4. Conclusion**

47  
48 Attribution of the IR bands of the carbonates adsorbed on MgO is a very important tool to  
49  
50 identify the nature of the active basic sites available after a pretreatment. DFT calculations  
51  
52 combined with the DRIFT measurement on MgO sample after peculiar pretreatments allow us  
53  
54 to give a new assignment to these IR bands considering the adsorption on (100) defects and  
55  
56 (110) and (111) planes. These attributions are confirmed by the thermodynamic calculations  
57  
58 of the stability of all carbonate species. Moreover, these results give a new tool to identify the  
59  
60

1  
2  
3 crystallographic plane and defects by analysing the formation of IR-band when absorbing the  
4  
5 CO<sub>2</sub> on it. Results show that the strongest basic site versus CO<sub>2</sub>, which is a Lewis acid, is not  
6  
7 the same that the strongest basic site for the deprotonating adsorption of Brønsted acids. Thus,  
8  
9 even of the same nature, Lewis and Brønsted basic sites differ by their basicity strength scale.  
10  
11 This conclusion should have consequences on the use of CO<sub>2</sub> TPD, when it has to be  
12  
13 correlated with kinetic studies of basic Brønsted reactivity.  
14  
15  
16  
17  
18  
19  
20  
21

22 **Acknowledgments:** The authors kindly wish to acknowledge David Loffreda for the  
23  
24 thermodynamic phase diagram calculations of adsorption of carbonates and Konstantin  
25  
26 Hadjiivanov, Françoise Delbecq, Frederik Tielens as well as Guylène Costentin for the  
27  
28 fruitful discussions. This work was granted access to the HPC resources of  
29  
30 [CCRT/CINES/IDRIS] under the allocation 2010 [x2010086395] made by GENCI (Grand  
31  
32 Equipement National de Calcul Intensif).  
33  
34  
35  
36  
37  
38  
39  
40  
41  
42  
43  
44  
45  
46  
47  
48  
49  
50  
51  
52  
53  
54  
55  
56  
57  
58  
59  
60

## References

- [1] Huber G.W.; Iborra S.; Corma A., *Chem. Rev.*, **2006**, *106*, 4044.
- [2] Busca G., *Chem. Rev.*, **2010**, *110*, 2217.
- [3] Corma A.; Iborra S, *Adv. in Catal.*, **2006**, *49*, 239.
- [4] Chizallet C.; Costentin G.; Che M.; Delbecq F.; Sautet P., *J. Phys. Chem. B* **2006**, *110*, 1587.
- [5] Chizallet C.; Costentin G.; Che M.; Delbecq F.; Sautet P., *J. Am. Chem. Soc.* **2007**, *129*, 129, 6442.
- [6] Wang Ch-M. ; Wang Y-D. ; Dong J.; Liu S.; Xie Z-X., *Comp. Theo. Chem.* **2011**, *974*, 52.
- [7] Mekhemer G.A.H.; Halawy S.A.; Mohamed M.A.; Zaki M.I., *J. Phys. Chem. B* **2004**, *108*, 13379.
- [8] Du H.; Williams C.T.; Ebner A.D.; Ritter J.A., *Chem. Mater.* **2010**, *22*, 3519.
- [9] Puriwat J.; Chaitree W.; Suriye K.; Dokjampa S.; Praserttham P.; Panpranot J., *Catal. Comm.*, **2010**, *12*, 80
- [10] Cairon O.; Guesmi H., *Phys. Chem. Chem. Phys.*, **2011**, *13*, 11430
- [11] Fukuda Y.; Tanabe K., *Bull Bull. Chem. Soc. Jpn.*, **1973**, *46*, 1616.
- [12] Smart R.S.C.; Slager T. L.; Little L.H.; Greenler, R. G., *J. Phys. Chem.*, **1973**, *77*, 1019.
- [13] Busca G.; Lorenzelli V., *Mater. Chem*, **1982**, *7*, 89.
- [14] Yanagisawa Y., Takaoka K., Yamabe S., Ito T., *J. Phys. Chem.*, **1995**, *99*, 3704.
- [15] Stark J.V.; Park D.G.; Lagadic I.; Klabunde K. J., *Chem. Mater.*, **1996**, *8*, 1904.
- [16]Kwon H., Park D. G., *Bull. Kor. Chem. Soc.* **2009**, *30*, 2567.
- [17] Mekhemer G. A. H., Halawy S. A., Mohamed M. A., Zaki M. I., *J Phys Chem B*, **2004**, *108*, 13379.
- [18] Menezes A. O., Silva P. S., Hernandez E. P., Borges L. E. P., Fraga M. A., *Langmuir*, **2010**, *26*, 3382
- [19] Du H., Williams C. T., Ebner A. D., Ritter J. A., *Chem. Mater.*, **2010**, *22*, 3519
- [20] Jensen M. B., Pettersson L. G. M., Swang O., Olsbye U., *J. Phys. Chem. B* **2005**, *109*, 16774
- [21] Hammamia R., Dhouiba A., Fernandez S., Minot C., *Catalysis Today*, **2008**, *139*, 227.



- 1  
2  
3  
4 [22] Preda G., Pacchioni G., Chiesa M., Giamello E., *J. Phys. Chem. C*, **2008**, *112*, 19568.  
5  
6 [23] Allen J.P., Parker S. C., Price D. W., *J. Phys Chem C* , **2009**, *113*, 8320  
7  
8 [24] Kim H. Y., Lee H. M., Park, J.-N, *J. Phys. Chem C*. **2010**, *114*, 7128  
9  
10 [25] Gay I.D., Harrison N.M., *Surf. Sc.* **2005**, *591* 13  
11  
12 [26] Kresse, G.; Hafner, J. *Phys. Rev. B* **1993**, 558.  
13  
14 [27] Kresse, G.; Hafner, J. *Phys. Rev. B* **1994**, *49*, 14251.  
15  
16 [28] Perdew J. P., Chevary J. A., Vosko S. H., Jackson K. A., Pederson M. R., Singh D. J.,  
17 Fiolhais C., *Phys. Rev. B* **1992**, *46*, 6671.  
18  
19 [29] Blochl P. E., *Phys. Rev. B* **1994**, *50*, 17953.  
20  
21 [30] Herzberg G., *Molecular Spectra and Molecular Structure*, second ed., Lancaster Press,  
22 Inc., Lancaster, PA, **1950**. p. 274.  
23  
24 [31] Petitjean H.; Tarasov K.; Delbecq F.; Sautet P.; Krafft J.-M.; Bazin P.; Paganini M.C.;  
25 Giamello E.; Che M.; Lauron-Pernot H.; Costentin G., *J.Phys. Chem. C* **2010**, *114*, 3008.  
26  
27 [32] Lazarov V.K. ; Plass R. ; Poon H-C., Saldin D.K.; Weinert M.; Chambers S.A.;  
28 Gajdardziska-Josifovska M., *Phys. Rev. B* **2005**, *71*, 115434.  
29  
30 [33] Zhang W.-B., Tang B.-Y., *J. Phys. Chem. C* **2008**, *112*, 3327  
31  
32 [34] Spagnoli D., Allen J.P., Parker S.C., *Langmuir*, **2011**, *27*, 1821  
33  
34 [35] Mackrodt, W.C., *Phys. Chem. Miner.* **1988**, *15*, 228-237.  
35  
36 [36] Refson, K. ; Wogelius. R. A. ; Eraser, D.G. ; Payne, M.C. ; Lee, M.H. ; Milman, V.,  
37 *Phys. Rev. B* 1995, *52*, 10832.  
38  
39 [37] Loffreda D., *Surf. Sci.*, **2006**, *600*, 2103.  
40  
41 [38] Fuchs R., *Phys. Rev. B*, **1978**, *18*, 7160.  
42  
43 [39] AlGhamdi, K., Hargreaves, J. S. J., and Jackson, S. D. In Jackson, S. D. Hargreaves, J. S.  
44 J., Eds.; *Metal Oxide Catalysis*; Wiley-VCH: Weinheim, Germany, **2009**; Vol. 2, p 819.  
45  
46 [40] Trionfetti C.; Babich I. V.; Seshan K.; Lefferts L., *Langmuir*, **2008**, *24*, 8220  
47  
48 [41] Arndt S. ; Laugel G.; Levchenko S.; Horn R. ; Baerns M.; Scheffler M.; Schlögl R.;  
49 Schomäcker R., *Catal. Rev*, **2011**, *53*, 424  
50  
51 [42] Pacchioni G., *Surf. Sci.*, **1993**, *281*, 207.  
52  
53  
54  
55  
56  
57  
58  
59  
60

- 1  
2  
3 [43] Scheffler, M.; Stampfl, C., Theory of adsorption on Metal substrates. In *Handbook of*  
4 *Surface Science, Vol. 2: Electronic Structure*; Horn, K.; Scheffler, M., Eds.; Elsevier:  
5 Amsterdam, 2000.  
6  
7  
8 [44] Vaspview. <http://vaspviewer.sourceforge.net/>.  
9  
10 [45] Saussey J., Lavalley J-C., Bovet C., *J. Chem. Soc., Faraday Trans.* **1982**, 78, 1457.  
11  
12 [46] Wander A.; Bush I.J.; Harrison N.M., *Phys. Rev.* **2003**, 68, 233405.  
13  
14 [47] Refson K.; Wogelius R. A.; Fraser D. G.; Payne M. C.; Lee M. H.; Milman V., *Phys.*  
15 *Rev. B*, **1995**, 52,10823.  
16  
17 [48] Hacquart R.; Jupille J., *J. of Cryst. Growth*, **2009**, 311, 4598.  
18  
19 [49] Evans J.V.; Whateley T. L., *Trans. Faraday Soc.*, **1967**, 63, 2769.  
20  
21 [50] Parker S.C.; de Leeuw N.H.; Redfern S. E., *Faraday Discuss.*, **1999**, 114, 381  
22  
23 [51] Weckhuysen B. M.; Mestl G.; Rosynek M. P.; Krawietz T. R.; Haw J. F.; Lunsford J. H.,  
24 *J. Phys. Chem. B*, **1998**, 102, 3773  
25  
26 [52] Krishnamurti D., *Proc. Math. Sci.* **1956**, 43, 210  
27  
28 [53] Hattori H., *J. Jap. Petrol. Instit.*, **2004**, 47, 67  
29  
30 [54] Lauron-Pernot H., *Catal. Reviews*, **2006**,48 ,315  
31  
32 [55] Brønsted J.N., *Rec. Trav. Chim. Pays-Bas*, **1923**, 42, 718  
33  
34  
35  
36  
37  
38  
39  
40  
41  
42  
43  
44  
45  
46  
47  
48  
49  
50  
51  
52  
53  
54  
55  
56  
57  
58  
59  
60

1  
2  
3  
4  
5  
6  
7  
8  
9  
10  
11  
12  
13  
14  
15  
16  
17  
18  
19  
20  
21  
22  
23  
24  
25  
26  
27  
28  
29  
30  
31  
32  
33  
34  
35  
36  
37  
38  
39  
40  
41  
42  
43  
44  
45  
46  
47  
48  
49  
50  
51  
52  
53  
54  
55  
56  
57  
58  
59  
60

## Tables:

**Table 1:** Review of the literature experimental attributions of IR-bands assigned to carbonates and hydrogen carbonates species adsorbed on MgO

### Hydrogen carbonates:

| $\nu_2$     | $\nu_3$     | $\nu_4$     | Work references |
|-------------|-------------|-------------|-----------------|
| 1655 – 1658 | 1405 – 1419 | 1220 – 1223 | [16]            |
|             | 1480        | 1250        | [15]            |
| 1650        | 1510,1408   | 1220        | [18]            |

### Carbonates:

| species     | $\nu_{3high}$ | $\nu_{3low}$ | $\nu_1$             | Work references |
|-------------|---------------|--------------|---------------------|-----------------|
| Monodentate | 1510 – 1550   | 1390 – 1410  | 1035 – 1050         | [16]            |
|             | 1550          | 1410         | 1050                | [11]            |
|             | 1520          | 1370         | 1060                | [12]            |
|             | 1590,1510     | 1415         |                     | [15]            |
| Bidentate   |               | 1385,1335    |                     | [15]            |
|             | 1659, 1626    | 1329, 1273   | 1024, 947           | [14]            |
|             | 1665 – 1710   | 1325 – 1330  | 1005 – 1030         | [16]            |
|             | 1670, 1630    | 1270         |                     | [12]            |
|             | 1670, 1630    | 1315, 1280   | 1000,850<br>950,830 | [11]            |

**Table 2:** Geometric (distances (Å) and angles (degrees °)), energetic ( $E_{\text{ads}}$  (eV)) and frequency values ( $\nu_{\text{CO}}$  ( $\text{cm}^{-1}$ )) of optimized  $\text{CO}_2$  species adsorbed on the (100) plan and its defects as well as the (110) and (111) surfaces. Values in brackets are reported from the literature

|                      | $E_{\text{ads}}$ (eV)                                 | O( $\alpha$ )-Mg (Å)                               | O( $\alpha$ )-C (Å)   | O( $\beta$ )-C (Å)  | O( $\gamma$ )-C (Å)                                | OCO (degree)  | $\nu_{3\text{h}}$ ( $\text{cm}^{-1}$ )             | $\nu_{3\text{l}}$ ( $\text{cm}^{-1}$ )             |
|----------------------|---|--|---|---|--|---|--|--|
| Terrace (T)          | -0.09   | 2.70   | 1.18  |   |  | 177.8   | 2346   | 1308   |
| Monoatomic step (S1) | -2.26   | 2.10   | 1.28  | 1.36  | -  | 129.9   | 1603   | 1300   |
| Diatomic step (S2)   | -2.16<br>(-1.58) <sup>a</sup><br>(-2.16) <sup>b</sup> | 2.09<br>(2.14) <sup>b</sup><br>(2.08) <sup>c</sup> | 1.27<br>(1.25) <sup>a</sup><br>(1.26) <sup>b</sup><br>(1.26) <sup>c</sup> | 1.38<br>(1.38) <sup>a</sup><br>(1.37) <sup>b</sup><br>(1.38) <sup>c</sup> | -  | 130.6<br>(130.6) <sup>a</sup><br>(131) <sup>b</sup> | 1639<br>(1784) <sup>a</sup><br>(1606) <sup>c</sup> | 1287<br>(1288) <sup>a</sup><br>(1237) <sup>c</sup> |
| Corner (C3)          | -1.53<br>(-1.18) <sup>a</sup><br>(-1.87) <sup>b</sup> | 1.95<br>(1.97) <sup>b</sup>                        | 1.31<br>(1.29) <sup>b</sup><br>(1.29) <sup>c</sup>                        | 1.40<br>(1.42) <sup>b</sup><br>(1.40) <sup>c</sup>                        | 1.24<br>(1.21) <sup>a</sup><br>(1.22) <sup>b</sup> | 126.9<br>(129) <sup>a</sup><br>(128) <sup>b</sup>   | 1727<br>(1778) <sup>b</sup>                        | 1198<br>(1243) <sup>b</sup>                        |
| Kink (K)             | -2.02   | 2.04   | 1.34  | 1.37  | 1.23   | 125.8   | 1679   | 1125   |
| Divacancy (D)        | -1.97   | 2.05   | 1.33  | 1.37  | 1.24   | 125.9   | 1649   | 1149   |
| (110)                | -2.75<br>-2.16 <sup>d</sup>                           | 2.08   | 1.28  | 1.34  | -  | 128.9   | 1559   | 1331   |
| (111)                | -0.79<br>(0.28) <sup>d</sup><br>(-3.97) <sup>f</sup>  |  | 1.31  | 1.31  | -  | 115.8   | 1440<br>(1572-<br>1631) <sup>f</sup>               | 1378<br>(1440 -<br>1459) <sup>f</sup>              |

Ref. <sup>a</sup>[20], <sup>b</sup>[22], <sup>c</sup>[14], <sup>d</sup>[24], <sup>f</sup>[23]

**Table 3 :** Calculated DFT adsorption energies (eV) and  $\nu_{3h}$  and  $\nu_{3l}$  IR vibrations ( $\text{cm}^{-1}$ ) for different coverage of carbonate species adsorbed on MgO(100) steps and MgO (110) and (111) surfaces. Values in brackets are reported from the literature

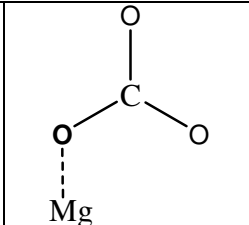
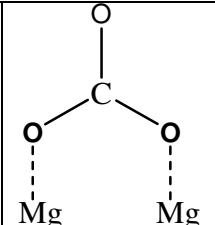
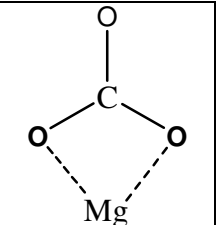
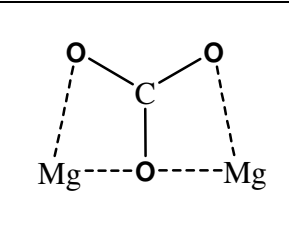
|                    | Coverage ML | $E_{\text{ads}}$ (eV) | $\nu_{3h}$ ( $\text{cm}^{-1}$ )                            | $\nu_{3l}$ ( $\text{cm}^{-1}$ )                         |
|--------------------|-------------|-----------------------|--|---|
| S1 (3 sites)       | 1/3         | -2.26                 | 1603   | 1300  |
|                    | 2/3         | -1.25                 | 1691, 1626<br>(1588-1638) <sup>G</sup>                     | 1284, 1259<br>(1520-1564) <sup>G</sup>                  |
|                    | 1           | -0.32                 | 1754, 1710, 1657   | 1260, 1255, 1248  |
| S2 (3 sites)       | 1/3         | -2.16                 | 1639   | 1287  |
|                    | 2/3         | -0.90                 | 1728, 1691   | 1280, 1262  |
|                    | 1           | +0.93                 | 1824, 1775, 1695   | 1284, 1235, 1224  |
| (110)<br>(9 sites) | 1/9         | -2.75                 | 1559   | 1331  |
|                    | 1/3         | -2.49                 | 1554, 1552, 1525   | 1316, 1302, 1301  |
|                    | 2/3         | -0.93                 | 1688, 1687, 1660, 1609,<br>1608, 1594                      | 1287, 1272, 1271, 1254,<br>1253, 1250                   |
|                    | 1           | +2,70                 | 1796, 1795, 1759, 1759,<br>1743, 1742, 1742, 1721,<br>1720 | 1270, 1258, 1258, 1252, 1252,<br>1251, 1251, 1246, 1246 |
| (111)<br>(9 sites) | 1/4         | -0.85                 | 1440   | 1378  |
|                    | 2/4         | -0,34                 | 1523, 1463   | 1399, 1236  |
|                    | 3/4         | +0,10                 | 1850, 1824, 1789   | 1161, 1077, 1034  |

Ref. <sup>G</sup>[43]

**Table 4** : Summary of experimental and theoretical data: Nomenclature, Desorption temperatures (K), and frequencies of all computed carbonate species adsorbed over MgO support.

| Face  | Type of carbonate | Type of defect | Nomenclature | experimental data           |                  |                  | DFT Calculations             |                |                |
|-------|-------------------|----------------|--------------|-----------------------------|------------------|------------------|------------------------------|----------------|----------------|
|       |                   |                |              | Desorption on DRIFT spectra | $\nu_{3h}$ DRIFT | $\nu_{3l}$ DRIFT | T (K) for $\Delta G_{ads}=0$ | $\nu_{3h}$ DFT | $\nu_{3l}$ DFT |
| (100) | Bidentate         | Corner         | B-C3         | 873 > T > 673 K             | 1680             | Out of range     | 722                          | 1650-1730      | 1125-1200      |
|       |                   | Kink           | B-K          | 873 > T > 673 K             |                  |                  | 822                          |                |                |
|       |                   | Divacancy      | B-D          | 873 > T > 673 K             |                  |                  | 812                          |                |                |
|       | Tridentate        | Step           | T-S1 T-S2    | T > 873 K                   | 1651             | 1304             | 908                          | 1600-1650      | 1280-1300      |
| (110) | Tridentate        |                | T-110        | 873 > T > 673 K             | 1516             | 1347             | 1212                         | 1560           | 1330           |
| (111) | Mono dentate      |                | M-111        | 873 > T > 673 K             |                  |                  | 314                          | 1440           | 1378           |

Scheme 1: Description of the carbonate species adsorbed on magnesium oxide according to the literature and as revisited in this study

|                 |   |   |  |   |
|-----------------|---|---|--|---|
|                 |  |  |  |  |
| Described as    | Monodentate [2], unidentate [6]   | Bridging [2,6]  | Bidentate [2,6]  | Polydentate [2] monodentate [15]  |
| Our description | Monodentate   | Bidentate   | Bidentate  | Tridentate  |

1  
2  
3 **Figure captions:**  
4  
5  
6  
7

8  
9 **Figure 1:** The different steps of thermal treatment of the MgO sample.  
10

11  
12  
13 **Figure 2:** DRIFT spectra of the adsorbed species over magnesium oxide before (red line) and  
14 after (black line) pre-treatment at 1023 K (arbitral unit for absorbance)  
15  
16  
17

18  
19  
20 **Figure 3:** Recorded DRIFT spectra of the adsorbed species over magnesium oxide after CO<sub>2</sub>  
21 adsorption under inert gas for different *temp* treatments (arbitral unit for absorbance)  
22  
23  
24

25  
26  
27 **Figure 4:** Optimized configurations of adsorbed carbonates over MgO(100) defects and  
28 MgO(110) and (111) surfaces. Red, gray and blue balls represent Oxygen, Magnesium and  
29 Carbon atoms, respectively. O<sub>β</sub> is the oxygen of the carbonate inserted in the magnesium  
30 oxide network, O<sub>α</sub> is the oxygen coming from CO<sub>2</sub> bonded to magnesium cation and O<sub>γ</sub> is the  
31 oxygen which doesn't make connection with the surface.  
32  
33  
34  
35  
36  
37  
38

39  
40  
41 **Figure 5:** 3D visualization of the *charge density difference* of tridentate (T-S1 and T-110),  
42 bidentate (B-C3 and B-K) and mondentate (M-111) carbonate species. Pertinent isosurface  
43 values =  $-3.7 \cdot 10^{-2} \text{ e}/\text{\AA}^3$  for T-S1 and T-110;  $-20 \cdot 10^{-2} \text{ e}/\text{\AA}^3$  for B-C3 and B-K;  $12 \cdot 10^{-2}$  for M-  
44  
45  
46  
47  
48  
49 111.  
50

51 **Figure 6 :** Minimum energy configuration of the adsorption of two carbonates over the  
52 stepped MgO(100) defects; As the S1 has 3 adsorption sites on the edge, the coverage is  
53 supposed to be 2/3 ML.  
54  
55  
56  
57  
58  
59  
60



1  
2  
3 **Figure 7** : Gibbs free energy diagrams (kJ/mol) at a constant pressure ( $P_{\text{CO}_2} = 0.001 \text{ Pa}$ ) as a  
4  
5 function of temperature K for adsorbed carbonates on different MgO surfaces and defects.  
6  
7  
8  
9  
10  
11  
12  
13  
14  
15  
16  
17  
18  
19  
20  
21  
22  
23  
24  
25  
26  
27  
28  
29  
30  
31  
32  
33  
34  
35  
36  
37  
38  
39  
40  
41  
42  
43  
44  
45  
46  
47  
48  
49  
50  
51  
52  
53  
54  
55  
56  
57  
58  
59  
60

## Figures

Figure 1

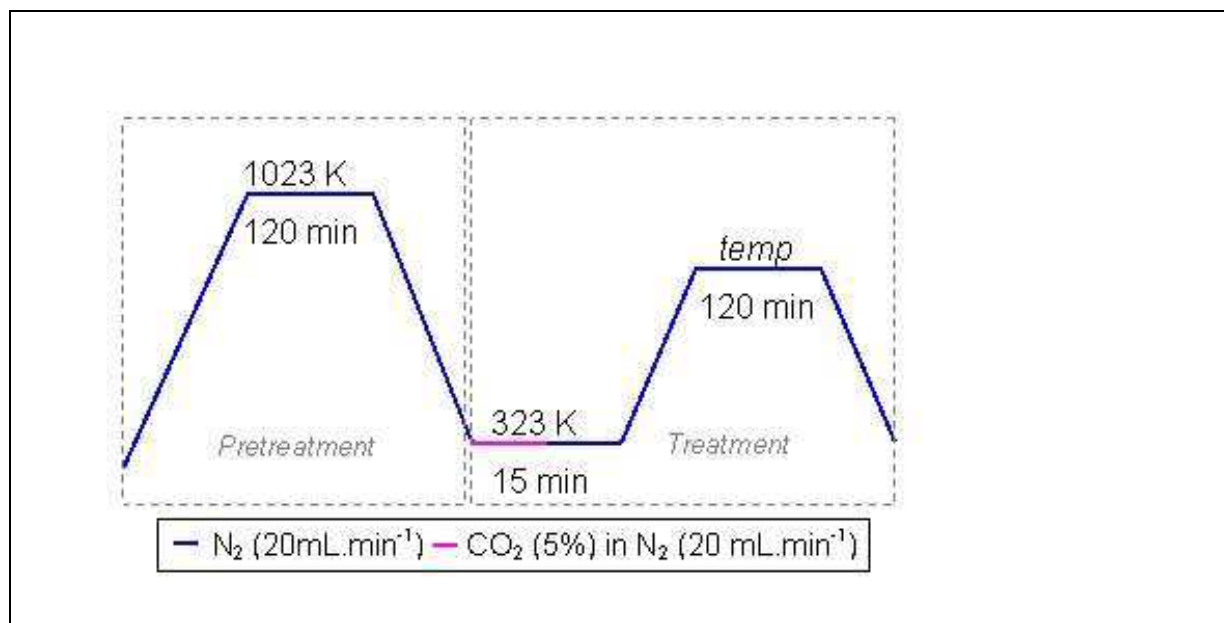


Figure 2

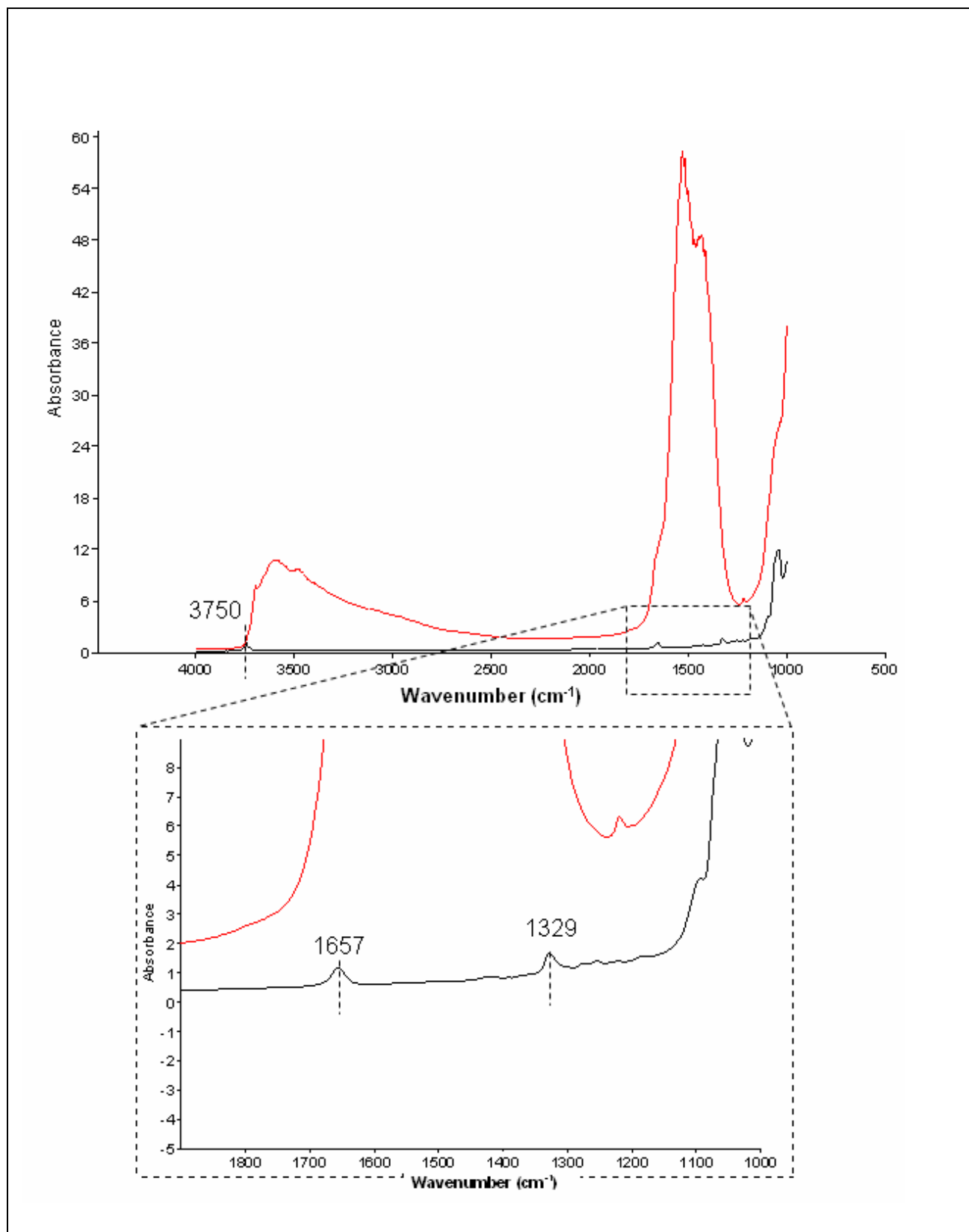


Figure 3

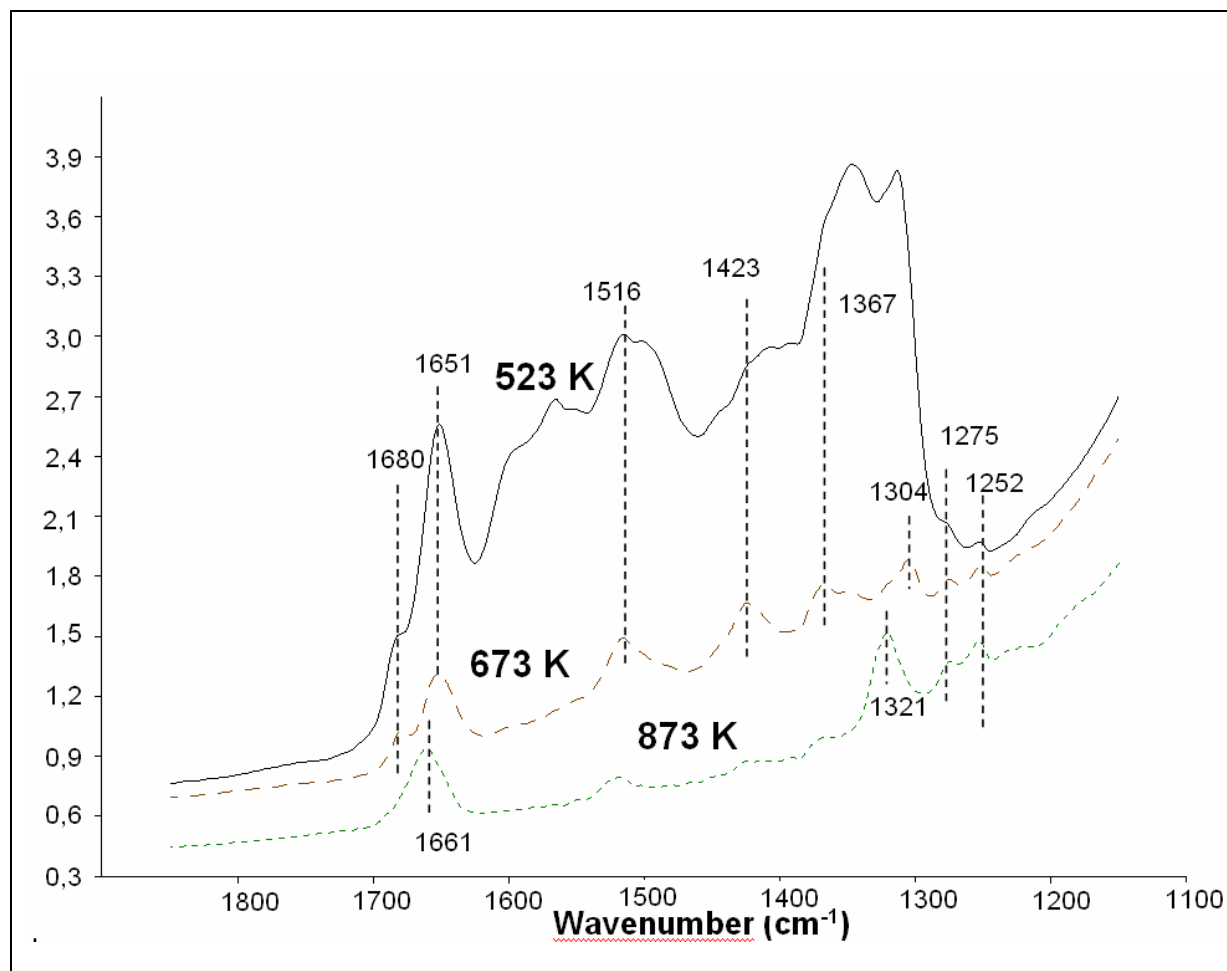


Figure 4

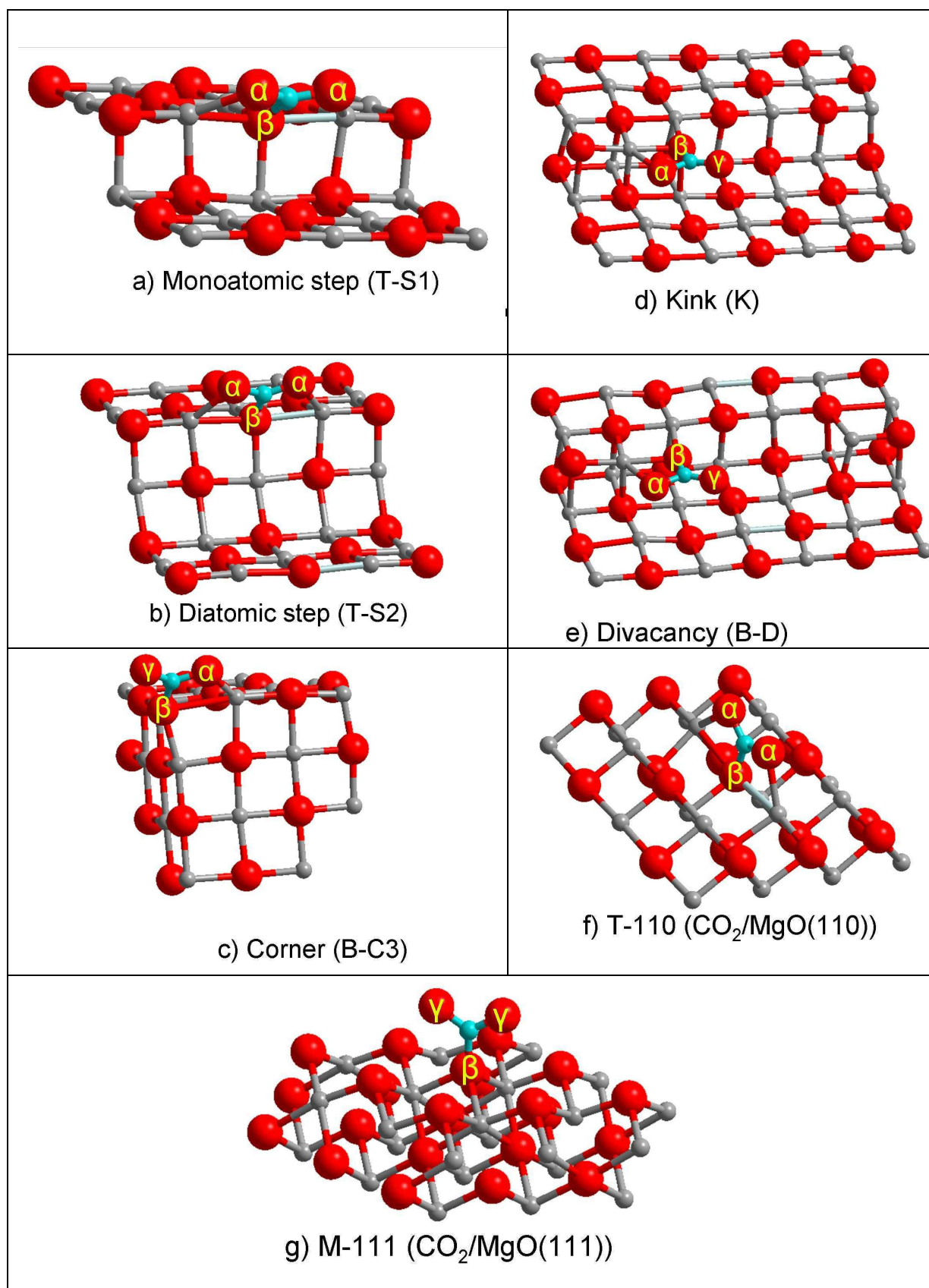


Figure 5

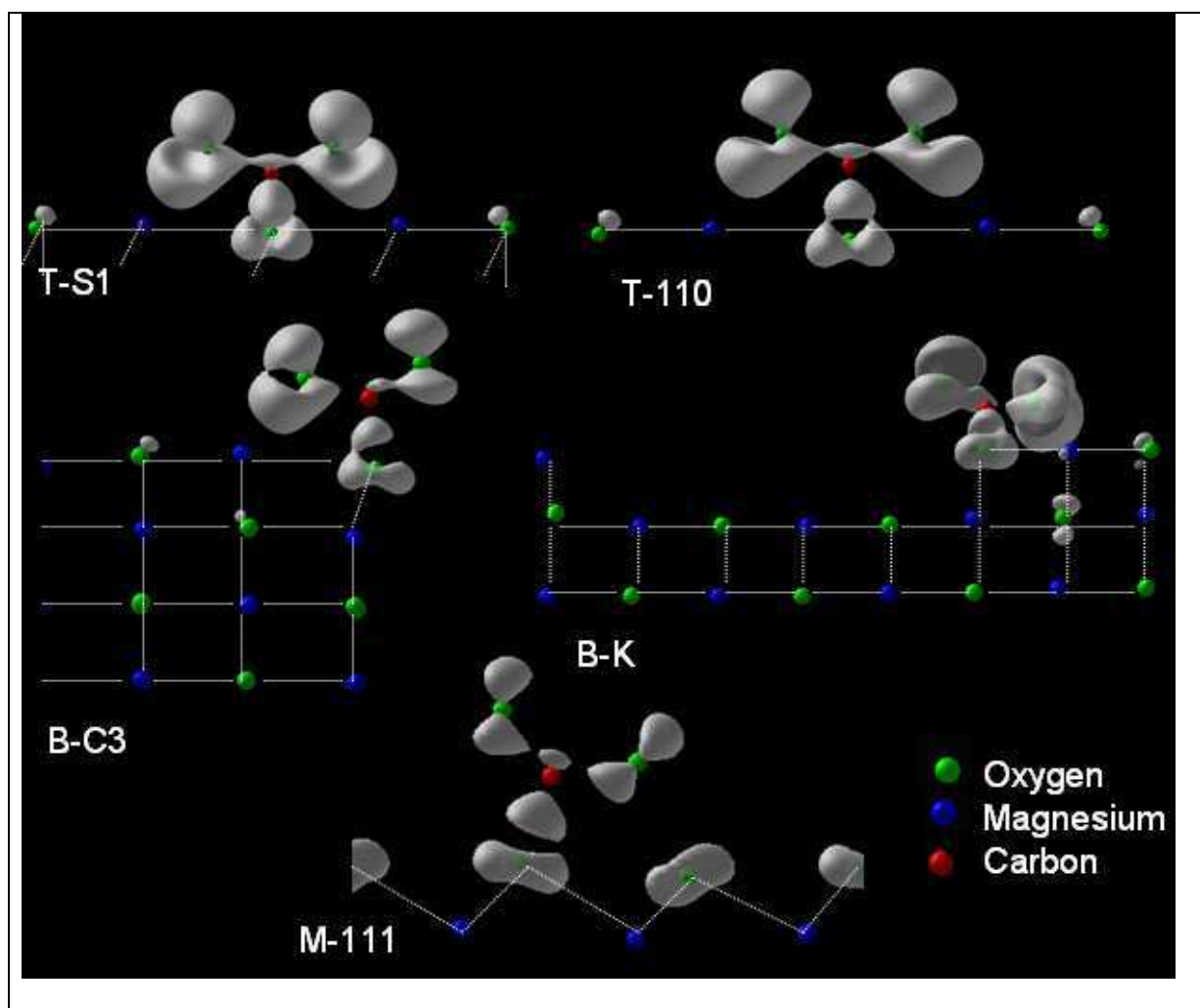


Figure 6

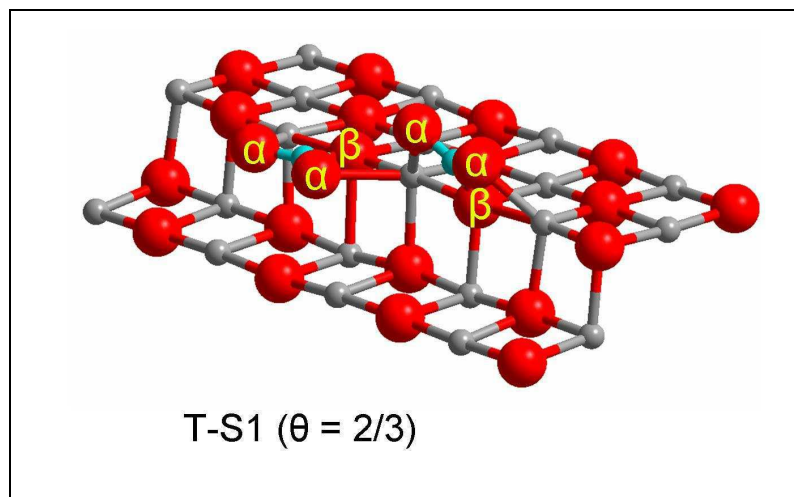
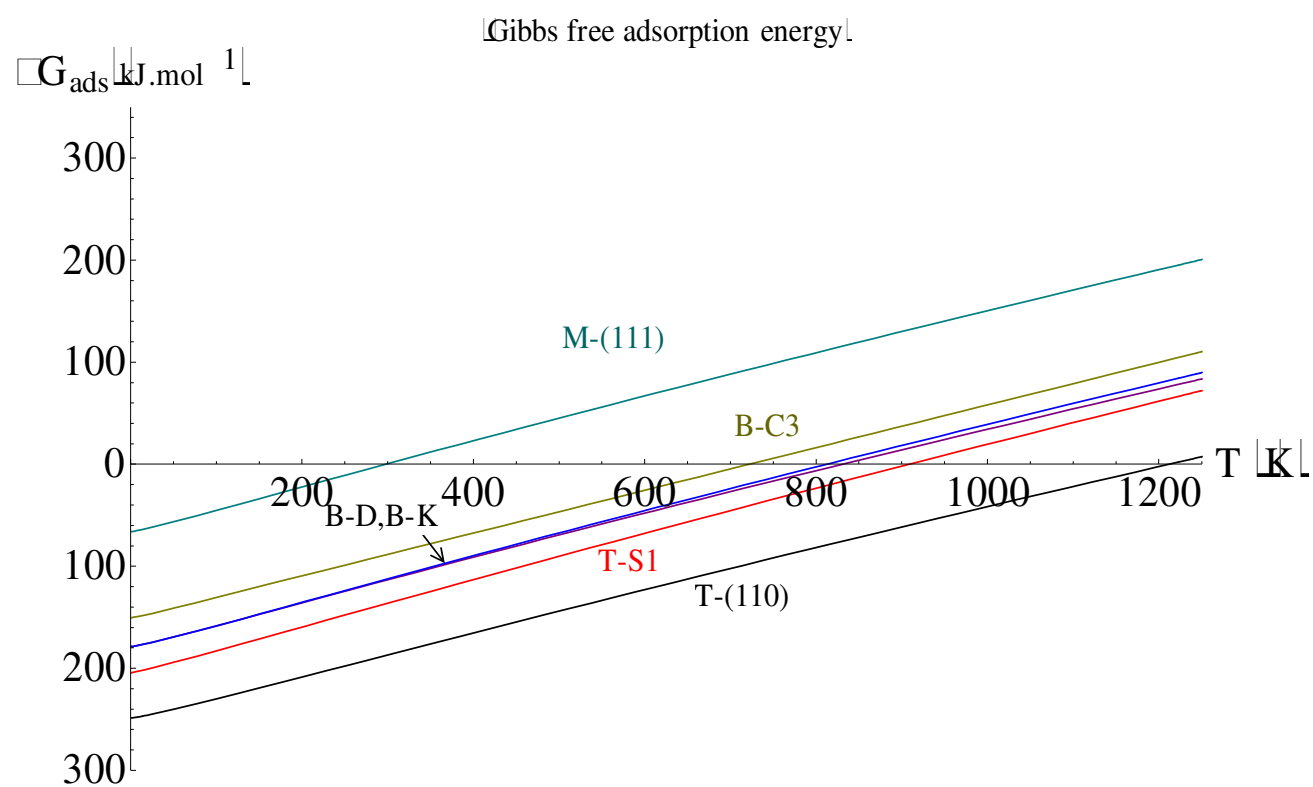


Figure 7





## The graphic for the TOC

